Phase-field simulation of texture evolution in magmatic rocks

Julia Kundin[1], Ingo Steinbach[1], and Sumit Chakraborty[2]

[1]Ruhr-University Bochum
[2]Ruhr-Universitat Bochum

November 22, 2022

Abstract

The tool of phase-field modeling for the prediction of chemical as well as microstructural evolution during crystallization from a melt in a mineralogical system has been developed in this work. We provide a compact theoretical background and introduce new aspects such as the treatment of anisotropic surface energies that are essential for modeling mineralogical systems. These are then applied to two simple model systems - the binary olivine-melt and plagioclase-melt systems - to illustrate the application of the developed tools. In one case crystallization is modeled at a constant temperature and undercooling while in the other the process of crystallization is tracked for a constant cooling rate. These two examples serve to illustrate the capabilities of the modeling tool. The results are analyzed in terms of crystal size distributions (CSD) and with a view toward applications in diffusion chronometry; future possibilities are discussed. The modeling results demonstrate that growth at constant rates may be expected only for limited extents of crystallization, that breaks in slopes of CSD-plots should be common, and that the lifetime of a given crystal of a phase is different from the lifetime of a phase in a magmatic system. The last aspect imposes an inherent limit to timescales that may be accessed by diffusion chronometry. Most significantly, this tool provides a bridge between CSD analysis and diffusion chronometry - two common tools that are used to study timescales of magmatic processes.

Phase-field simulation of texture evolution in magmatic rocks

J. Kundin[1], I. Steinbach[1], S. Chakraborty[2]

[1]Interdisciplinary Centre for Advanced Materials Simulation (ICAMS), Ruhr-University Bochum, D-44801 Bochum, Germany

[2]Institut of Geology, Mineralogy and Geophysics, Ruhr-University Bochum, D-44801 Bochum, Germany

Key Points:

- Phase-field modeling
- Crystal size distribution (CSD)
- Diffusion chronometry

Corresponding author: Julia Kundin, `julia.kundin@rub.de`

Abstract

The tool of phase-field modeling for the prediction of chemical as well as microstructural evolution during crystallization from a melt in a mineralogical system has been developed in this work. We provide a compact theoretical background and introduce new aspects such as the treatment of anisotropic surface energies that are essential for modeling mineralogical systems. These are then applied to two simple model systems - the binary olivine-melt and plagioclase-melt systems - to illustrate the application of the developed tools. In one case crystallization is modeled at a constant temperature and undercooling while in the other the process of crystallization is tracked for a constant cooling rate. These two examples serve to illustrate the capabilities of the modeling tool. The results are analyzed in terms of crystal size distributions (CSD) and with a view toward applications in diffusion chronometry; future possibilities are discussed. The modeling results demonstrate that growth at constant rates may be expected only for limited extents of crystallization, that breaks in slopes of CSD-plots should be common, and that the lifetime of a given crystal of a phase is different from the lifetime of a phase in a magmatic system. The last aspect imposes an inherent limit to timescales that may be accessed by diffusion chronometry. Most significantly, this tool provides a bridge between CSD analysis and diffusion chronometry - two common tools that are used to study timescales of magmatic processes.

1 Introduction

Physical chemistry is used to quantify the reading of the rock record to decipher processes that took place in and on the Earth. Thermodynamic analysis of complex chemical systems that correspond to bulk chemistry of diverse igneous and metamorphic rock types is now commonplace. Such analyses predict the stable mineral assemblages as well as the modal abundance and composition of the minerals as a function of intensive thermodynamic variables such as pressure, temperature, and fugacities of various species (e.g. f_{O_2}, f_{H_2O}). Petrological attributes of the rock record also include textural and microstructural characteristics, but a quantitative thermodynamically consistent approach to handle that is not yet available.

The situation is analogous to kinetic analysis. Studies of processes such as diffusion, nucleation, or crystal growth address these processes in individual mineral systems, or populations of crystals in some cases (e.g. nucleation and growth in molten systems), but in a manner that is generally decoupled from quantitative thermodynamic phase relations. In the best of cases, modeling efforts include alternating updates of thermodynamic and kinetic parameters, but without a means of ensuring physico-chemical consistency between these. Previous models for the simulation of texture evolution during crystallization processes in rocks were stochastic approaches, which were developed to validate theoretical models of the crystal size distribution with constant growth rates and an exponential nucleation rate (Marsh, 1988; R. V. Amenta, 2001, 2004; R. Amenta et al., 2007; Hersum & Marsh, 2006, 2007; Spillar & Dolejs, 2015). However, these models do not take into account thermodynamic conditions and operate with artificially imposed growth rates.

The emerging tool of phase-field (PF) modeling and analysis provides a means of addressing these problems (Langer, 1980; Karma, 2001; Boettinger et al., 2002; Chen, 2002; Steinbach, 2009; Kundin et al., 2015; Kundin & Steinbach, 2019). Notably, the method considers the energetics of surfaces and interfaces to couple these with more regularly considered bulk volume properties. The minimization of overall free energy taking these aspects into account allows the calculation of not only the stable configurations of solids and liquids in terms of their chemistry and abundance but also geometrical features such as grain size, shape, and distribution. Thus, commonly used tools such as crystal size

distribution (CSD) may be placed on a more quantitative foundation than has been possible until now.

As a tool, the phase-field method has hardly been applied to mineralogical systems. In this work, we introduce and develop the tool for some simple mineralogical systems to illustrate the approach and its possibilities. We begin by describing the theoretical background of the model. This part includes some newer developments that are more relevant for mineralogical systems, such as the exploration of the role of anisotropy of surface / interfacial energies in non-cubic systems. This is followed by some examples of numerical calculations of growth/ dissolution of faceted crystals in selected systems (plagioclase – melt and olivine – melt). We conclude by discussing some implications of our results for real geological systems, comparisons with currently available models of CSD-analysis, and considering some potential future applications.

2 Phase-field method

2.1 Phase field and diffuse interface

A complete phase-field (PF) method calculation includes a thermodynamic module (calculation of phase equilibria and deviations from equilibrium), a diffusion module (calculation of transport timescales), and an interface module that accounts explicitly for interfacial energies, i.e. capillarity. The last module permits the modeling of mobile interfaces between different phases or crystals of different orientations, and thereby, the evolution of microstructures and textures. This aspect is responsible for the novelty of the tool. In the following, a brief introduction is provided to how interfaces are handled, and references to works where more details may be found are provided, followed by a description of the method used in this study.

The method is based on two basic concepts: "Phase field" and "Diffuse interface". The Phase field is a field in space and time of an order parameter (usually denoted by $\phi(\mathbf{x}, t)$) that indicates the phase state of the system at each point within the (heterogeneous) volume of interest (see Fig. 1). Knowing the phase state (as indexed by the phase-field variable) one easily determines its properties of interest (chemical composition, state of strain, geometry of grain boundaries, etc.). The phase fields themselves evolve in time based on the demand for minimization of the free energy of the system. This aspect leads to a few major advantages that make Phase-field models particularly useful: (a) the evolution of the system occurs while maintaining internal thermodynamic consistency, (b) interfaces between grains and phases, which are indexed by individual phase fields ϕ_α, $\alpha = 1...N$ for N grains belonging to the same, or different crystallographic phases, do not need to be tracked individually, (c) grains of different orientations can be modeled separately by their "own" phase-filed parameters, and (d) one deals with scalar quantities rather than vectors with multiple components (see below for more on this). "Diffuse interface" is a phenomenological approach where an interface (say, between two crystals, or a crystal and a liquid) is considered to possess a finite width instead of being sharp. In terms of energetics, the consequences are that (a) the interface is a region of finite extent, (b) the interface can possess its "own" properties (e.g. diffusivity) that are distinct from those of the phases bounding an interface, and (c) the phase fields vary smoothly across the boundary and may be represented by continuous, differentiable functions, rather than show a discontinuity at the interface (where the property "jumps" from the value in one phase to that in the adjacent phase). The third aspect provides the fundamentally important characteristic that the gradient of a phase field (which is defined as a differentiable function) can be related to the velocity of an interface quantitatively in a thermodynamically consistent manner.
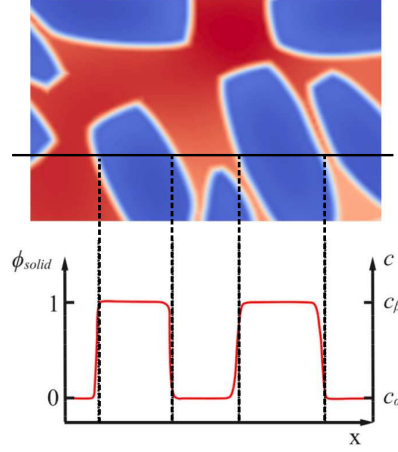
Figure 1. Scheme of a solidifying mush (upper part, solid in black, liquid in white). Measuring the composition along the line scan gives the saw tooth thread profile as displayed in the lower part of the figure, alternating between the composition in solid, c_β, and liquid, c_α. Normalizing this profile between 0 and 1 gives the phase-field profile $\phi(x)$. Note that we have drawn the profile in the interface in a "diffuse" manner, with an artificial width compared to the atomistic scale of a real interface. Consequently, the phase field shows a diffuse profile between the phases.

2.2 Free energy functional

A key aspect of the "diffuse interface" models is that they are based on a free energy functional which depends not only on the properties at a given point in the system but also on the local gradient of the phase field around that point

$$\mathcal{F} = \int_V \left[\frac{\epsilon^2}{2} |\nabla \phi|^2 + f_0(\phi) \right] dV. \tag{1}$$

Here, in some constant, non-homogeneous, reference volume V, $\mathcal{F}$ is the total Gibbs or Helmholtz Free Energy Functional of the system. It is composed of the sum of free energy per constituent of the homogeneous system, $f_0(\phi)$, and the contribution due to the inhomogeneity, $\frac{\epsilon^2}{2}(\nabla\phi)^2$. The inhomogeneity is also called the "gradient energy." Roughly speaking, it is a measure of the energy barrier for transformation between the phases and related to the interface energy as well as the driving force for transformation, see below. ϵ is the gradient energy coefficient, which is also related to the interface energy between grains of different orientations or of different phases.

Equation (1) was originally introduced by Landau (Hohenberg & Halperin, 1977) to describe the phase transition in superconductivity. Then it was introduced by Cahn and Hilliard (1958) to describe the phase transformation in particular for spinodal decomposition. Later Kobayashi (1993) introduced the model for dendrite solidification in metals where $f_0(\phi)$ is constructed as a sum of two terms: the potential, $f^{DW}(\phi)$ and the driving force for phase transformation Δg multiplied with the model function $h(\phi)$:

$$f_0(\phi) = \frac{\gamma}{4} f^{DW}(\phi) + \Delta g \, h(\phi). \tag{2}$$

$f^{DW}(\phi)$ is responsible for phase separation and the creation of the interface since it penalizes intermediate values of the phase field $0 < \phi < 1$ with an energy proportional to the positive material parameter, γ. Here the original form of a double well potential

$f^{DW}(\phi) = \phi^2(1-\phi)^2$ is used. $\Delta g\, h(\phi)$ is the chemical energy part, which is responsible for the driving force of the phase transformation between phases with a bulk energy difference Δg and a coupling function $h(\phi) = \phi^2(3-2\phi)$ which varies monotonously between 0 and 1. The functional (1) reads, translated in physical units (for details see appendix of (Steinbach, 2009)):

$$\mathcal{F} \int_V \left[\frac{\sigma}{\eta} \left(\frac{\eta^2}{2}|\nabla\phi|^2 + 18\phi^2(1-\phi)^2 \right) - \Delta g\phi^2(3-2\phi) \right] dV. \tag{3}$$

Here σ is the interface energy in units of energy per area, η is the interface width, Δg, as before, the bulk energy difference between the equilibrium and non-equilibrium state in units of energy per volume and $h(\phi)$ is the coupling function. A main feature of the functional is that the energy $f_0(\phi)$ has local minima in the liquid and in the solid phases at $\phi = 0$ and 1. The first term (gradient) and the second term (potential) contribute to the interface energy, in particular, the surface energy between liquid and solid phases. The illustration of the functional terms is shown in Fig. 2. One important aspect is that for the minimum solution of the phase field, the gradient and the potential terms show identical forms ($|\nabla\phi|^2 = \frac{36}{\eta^2}\phi^2(1-\phi)^2$). The proof for this is also given in the appendix of Steinbach (2009).
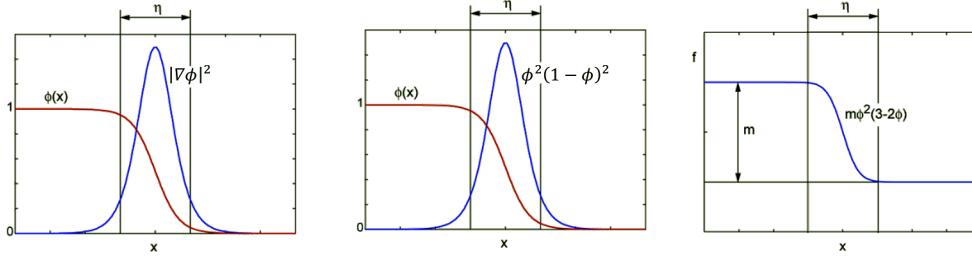

Figure 2. Mesoscopic interpretation of the free energy functional. From left to right the subsequent panels illustrate the first second and third terms in eq. (3), η is the interface width.

Depending on the application one may start from different thermodynamic functionals such as the Helmholtz free energy, or the Gibbs free energy. Here we treat only problems of phase transformations with fixed temperature and pressure and therefore we use the Gibbs free energy. The chemical part of the free energy density Δg is, in general, defined by the total Gibbs energy of a material point composed of different phases and depends on the composition (in simple binary systems it is simply the concentration c). It has been typically taken from thermodynamic databases such as CALPHAD (Lukas et al., 2007) for many metallic systems and ceramics and may be connected to databases such as MELTS (M. S. Ghiorso, n.d.; S. R. O. Ghiorso Mark S., 1995) for mineral-melt systems.

2.3 Evolution equations

The introduction of the gradient of the phase field in the energy functional makes the formulation non-local and allows changes in the environment of a point to influence the evolution of the system. With this aspect, the time evolution of the order parameter is governed by the demand for free energy minimization, called the "time-dependent Ginzburg-Landau models" (here written for a single phase field, the generalization to multiple phases will be presented in section 2.7):

$$\dot{\phi} = -M_\phi \frac{\delta\mathcal{F}(\phi)}{\delta\phi}. \tag{4}$$

139 Here M_ϕ is the interface mobility with units of inverse time multiplied by inverse energy
140 density.

In the same way, we can write down the evolution equation for concentration, which
is a conserved order parameter. This equation also referred to as the Cahn Hilliard equation (Cahn & Hilliard, 1958)

$$\dot{\phi} = \nabla M_c \nabla \frac{\delta \mathcal{F}(c)}{\delta c}, \tag{5}$$

141 where M_c is an atomic mobility.

In more technical terms, conserved quantities (e.g. mass or concentration) are treated
using eq. (5) and non-conserved quantities (e.g. phase-field order parameters, geometrical properties – Euler angles to characterize interfaces) are treated using eq. (4). The
calculation of the temporal evolution of a system requires the use of derivatives of the
free energy in the above form, leading to the use of functionals (roughly, a function of
a function) and variational derivatives which are defined as

$$\frac{\delta \mathcal{F}}{\delta \phi} = \frac{\partial f}{\partial \phi} - \nabla \cdot \frac{\partial f}{\partial \nabla \phi}, \tag{6}$$

142 where f is the energy density which is under the sign of the volume integral in eq. (1).

143 The equation of motion for a non-conserved order parameter (4) with the functional
144 (1) and (3), now referred to as the time-dependent Ginzburg-Landau models, is also known
145 as the Allen-Cahn equation (Allen & Cahn, 1979). Cahn and Hilliard (1958) first stud-
146 ied systems with locally uniform stable states and a conserved order parameter. The cor-
147 responding equation of motion (5) which is based on the Onsager relations (Onsager, 1931)
148 is known today as the Cahn-Hilliard equation. Details may be found also in (Wang et
149 al., 1993; Steinbach, 2009; Cheng et al., 2012).

Applying Eq. (4) to the functional (3), we obtain

$$\dot{\phi} = \mu \left[\sigma \left(\nabla^2 \phi + \frac{36}{\eta^2} \phi (1-\phi)(2\phi - 1) \right) - \frac{6}{\eta} \Delta g \, \phi (1-\phi) \right]. \tag{7}$$

150 The first two terms within the brackets correlate to the curvature of the interface, the
151 last term is the transformation driving force. The evolution equation in the steady-state
152 case without driving force, $\dot{\phi} = 0$, has the solution in one dimension, which gives the
153 tangential form of the diffuse interface (see Fig. 2).

154 Here we define new interface mobility $\mu = \eta M_\phi$ with units of velocity multiplied
155 by inverse energy density. Note that for the double obstacle potential $\mu = \dfrac{8\eta}{\pi^2} M_\phi$.

2.4 Interface mobility

The phase-field models define the velocity of the moving interface by the so-called
Gibbs-Thomson equation, which relates the velocity of the interface to the kinetic undercooling (Steinbach, 2009; Karma, 2001)

$$v_n = \mu (\Delta g - \sigma \kappa). \tag{8}$$

157 Here, v_n is the velocity in the direction normal to the interface at a given point, μ is mo-
158 bility, σ is the interfacial energy for isotropic systems, Δg is the constant part of the ther-
159 modynamic driving force and κ is the mean curvature of the interface.

160 Expression for the interface mobility, μ, of a solid-liquid interface for a diffusion-
161 controlled process (in this case the physical interface mobility is expected to be high) was
162 given by Karma and Rappel (1998); Steinbach (2009); Kundin and Steinbach (2019). For
163 interface-controlled processes, the physical interface mobility is expected to be smaller
164 and μ may be estimated by making use of the Gibbs-Thomson equation.

In the case of pure grain growth, the grain boundary energy and the grain boundary mobility can be estimated from kinetic coefficients K that are measured in experiments on growth kinetics (average grain size versus time):

$$K = \gamma \mu \sigma, \tag{9}$$

where γ is a constant, which depends on the form of grains, $\mu\sigma$ is called the "reduced interface mobility".

2.5 Thermodynamic driving force

The thermodynamic driving force for a phase transformation is defined as the slope of the Gibbs energy versus the progress of the transformation, $\Delta g = \frac{\partial G}{\partial \xi}$. In the phase-field model ξ is the phase-field order parameter. Using the mass conservation law in the form of a mixture concentration

$$c = c_\alpha \phi + c_\beta (1 - \phi), \tag{10}$$

where c_α is the phase concentration in the α phase, and the Lagrange multiplier method, one can write the Gibbs energy as a function of the phase-field order parameter

$$g = g_\alpha \phi + g_\beta (1 - \phi) + \mu^{eq}(c - c_\alpha \phi - c_\beta(1 - \phi)), \tag{11}$$

where g_α is the Gibbs energy density in the α phase. The derivative of g versus ϕ gives the driving force as the difference in diffusion potentials,

$$\Delta g = g_\alpha - g_\beta - \mu^{eq}(c_\alpha - c_\beta) = (c_\alpha - c_\beta)(\mu - \mu^{eq}), \tag{12}$$

where $\mu = \dfrac{g_\alpha - g_\beta}{c_\alpha - c_\beta}$ is a non-equilibrium diffusion potential and $\mu^{eq} = \dfrac{\partial g_\alpha}{\partial c_\alpha} = \dfrac{\partial g_\beta}{\partial c_\beta}$ is a quasi equilibrium diffusion potential. The driving force between liquid and solid phases can be expressed in terms of the entropy change on melting as:

$$\Delta g_{LS} = \Delta S_{LS} m_L (c_L - c_L^{eq}), \tag{13}$$

where ΔS_{LS} is the entropy change between liquid and solid phases, m_L is the liquidus slope (Eiken et al., 2006).

2.6 Anisotropy of surface energy

Grain boundary energies of only a few minerals are known, but it is now becoming possible to calculate grain boundary energies for different crystals using ab-initio simulations, and some examples in the material science literature include (Lee & Choi, 2004; Kim et al., 2011).

For faceted crystals, the growth velocity is inversely proportional to the surface energy for a particular facet. The surface energy anisotropy (the dependency of growth rate on the crystal plane) can be estimated using different experimental methods, for example: (i) using experimental crystal growth velocity in different crystal directions, (ii) the relative values of the surface energy for different faces can also be estimated using the shape of the crystal. The distance from the center to a crystal face is proportional to the surface energy, (iii) The absolute value of surface energy can be calculated by atomistic methods (e.g. ab-initio calculations). The surface energy of olivine was calculated, for example, by de Leeuw et al. (2000); Bruno et al. (2014). (iv) There are also experimental methods for the definition of grain boundary anisotropy based on the relative abundance of different grain boundary planes in an aggregate (e.g. see Saylor et al. (2000) for an example in MgO, and Marquardt et al. (2015) for olivine). A single experimental study is available on the measurement of interfacial energy between olivine and a basaltic melt (Cooper & Kohlstedt, 1982).

In the anisotropic model used in the present work, the surface or grain boundary energies in eqs. (7) and (8) change to the stiffness, σ^*. Due to anisotropy, the surface energy in the functional (3) is a function of an inclination angle θ, which is the angle between a crystal direction in a crystal lattice and the normal to the interface $\mathbf{n} = \nabla\phi/|\nabla\phi|$. Hence, $\sigma(\theta)$ is a function of gradients, $\nabla\phi$, and by means of eq. (6), it transforms to the 'stiffness' $\sigma^*(\theta) = \sigma + \sigma''$, where σ'' is the second derivative of σ with respect to θ. Note that the stiffness as well as the surface energy is a characteristic of each face of a crystal.

2.7 Multi-phase-field model

The multi-phase field model is described in details in the work of Steinbach (2009). The model can treat an arbitrary number of crystals by using a set of phase-field variables $\phi_\alpha(\mathbf{x}, t)$, limited only by available computer resources. As before, phase-field order parameters are defined as $\phi_\alpha = 1$ in the bulk α phase and $\phi_\alpha = 0$ in other phases.

The time evolution of phase-field parameters in the multi-phase formalism is constructed following eq. (4) as a sum over all dual interactions between the phases

$$\dot{\phi}_\alpha = -\sum_{\beta=1}^{\tilde{N}} \frac{M_{\alpha\beta}}{\tilde{N}} \left(\frac{\delta\mathcal{F}}{\delta\phi_\alpha} - \frac{\delta\mathcal{F}}{\delta\phi_\beta} \right), \tag{14}$$

where $M_{\alpha\beta}$ is the interface mobility, defined separately for each pair of phases, $\tilde{N}$ is number of phases on the interface. In a contact point, we have to treat $\tilde{N}$ phases simultaneously, $\tilde{N} = 3$ for a triple junction, $\tilde{N} = 4$ for a quadruple junction and so on.

3 Multi-phase-field model adopted for the simulations of the olivine and plagioclase crystal growth

3.1 Governing equations

In the present study, the multi-phase field model of Steinbach (2009) has been applied using the open source library *OpenPhase* (ICAMS, Department "Scale Bridging and Thermodynamic Simulation", Ruhr-Universtuy Bochum, n.d.). Here we consider a monomineralic system with $N-1$ crystals with the same phase but different orientations growing in a liquid phase. The crystals can come in contact with each other and form solid-solid interfaces of different misorientations. Individual orientations of crystals are defined in 3D by three Euler angles.

The free energy of a multi-phase system with N phase-field order parameters is formulated based on the Ginzburg-Landau functional eq. (1)

$$\mathcal{F} = \int_V \left(\sum_{\alpha \neq \beta}^N \frac{4\sigma_{\alpha\beta}}{\eta} \left\{ -\frac{\eta^2}{\pi^2} \nabla\phi_\alpha \cdot \nabla\phi_\beta + \phi_\alpha\phi_\beta \right\} \right.$$
$$\left. + \frac{X(T)}{2} \left(c - c^{eq}(T) \right)^2 \right) dV, \tag{15}$$

where the first two terms within the brackets set the interface energy $\sigma_{\alpha\beta}$ between the phase fields ϕ_α and ϕ_β, the second term within the brackets is the double obstacle potential, and the last term is the chemical part which depends on concentrations and temperature T (as well as pressure, P, in principle, but variations of P are not considered in this study).

The chemical part of the free energy density is the total Gibbs energy of the phases and is defined as a parabolic function of the chemical composition (Kundin et al., 2015). Here, c is the mixture concentration, c^{eq} is the equilibrium concentration of the mixture,

defined as a weighted sum on the interface

$$c^{eq} = c_S^{eq} \sum_{\alpha \neq L}^{N} h_\alpha(\phi_\alpha) + c_L^{eq}(1 - \sum_{\alpha \neq L}^{N} h_\alpha(\phi_\alpha)), \tag{16}$$

where c_S^{eq} and c_L^{eq} are equilibrium concentrations in solid and liquid phases, $h_\alpha(\phi_\alpha)$ is a special model function whose derivative over ϕ_α is $\partial h_\alpha/\partial \phi_\alpha = \sqrt{\phi_\alpha(1-\phi_\alpha)}$, that appears further in eq. (19). The full definition of $h(\phi)$ is given in the work of Steinbach (2009). The sum in eq. (16) is taken over all $N-1$ solid grains, which are the crystals of the same solid phase and have the same equilibrium concentration but different orientations. Furthermore, X is the mixture thermodynamic factor which is defined as a weighted sum

$$X = \left(\frac{1}{X_S}\phi_S + \frac{1}{X_L}(1 - \phi_S) \right)^{-1} = \frac{X_L}{k\phi_S + (1 - \phi_S)} \tag{17}$$

with X_L, X_S being the thermodynamic factors of liquid and solid phases, $\phi_S = \sum_{\alpha \neq L}^{N} \phi_\alpha$ being the sum of all solid phases on a space point, $k = X_L/X_S$ is the partition coefficient. It can be seen that X becomes X_L in the liquid and X_S in the solid phase.

In the olivine system considered in this study, the temperature is assumed to be homogeneous and constant during simulation. In the plagioclase system, the cooling rate is constant and cooling is considered as series of isothermal steps (see contrasting examples of olivine vs. plagioclase below). The binary phase diagrams are linearized , i.e., the slopes of the liquidus and solidus are approximated as linear within the range of interest with a partition coefficient, k, that describes the distribution of components between a solid and a coexisting liquid (i.e., $k = c_S/c_L$ at equilibrium). With these approximations, the equilibrium concentration c_α^{eq} in a phase α at a temperature T is calculated as

$$c_\alpha^{eq} = c_\alpha^{eq}(T_0) + \frac{(T - T_0)}{m_\alpha}, \tag{18}$$

where $m_\alpha = \partial T/\partial c_\alpha^{eq}$ and T_0 is the liquidus temperature. The linear dependency can be also changed to non-linear functions corresponding to the specifics of any phase diagram.

After substitution of the functional (1) in eq. (14), we obtain the resulting kinetic equation for a phase field

$$\dot{\phi}_\alpha = \sum_{\beta \neq \alpha}^{\tilde{N}} \frac{\mu_{\alpha\beta}}{\tilde{N}} \left(\sum_{\gamma \neq \alpha,\beta}^{\tilde{N}} [\sigma_{\beta\gamma}^* - \sigma_{\alpha\gamma}^*] \left[\nabla^2 \phi_\gamma + \frac{\pi^2}{\eta^2}\phi_\gamma \right] \right.$$
$$\left. + \frac{\pi}{\eta}\Delta g \sqrt{\phi_\alpha(1-\phi_\alpha)} \right). \tag{19}$$

The mobility $\mu_{\alpha\beta}$ is related to $M_{\alpha\beta}$ in eq. (14) as $\mu_{\alpha\beta} = \frac{8\eta}{\pi^2}M_{\alpha\beta}$. In this paper, we have used constant mobility for all interfaces, i.e., $\mu_{\alpha\beta} = \mu$. Of course, different mobilities of different interfaces can have a strong influence on the shapes of crystals and the evolution of the microstructure - this could be explored in a future study. The method can be consistently extended to provide various driving forces, address different extents of anisotropic surface energy, and to consider various grain boundary effects.

Here Δg is the thermodynamic driving force introduced above, which is the derivative over the phase-field variables of the chemical part of the free energy.

$$\Delta g = \frac{X_L(c_S^{eq} - c_L^{eq})(c - c^{eq})}{k\phi_S + (1 - \phi_S)} = \frac{\Delta S m_L(c - c^{eq})}{k\phi_S + (1 - \phi_S)}. \tag{20}$$

248 $\Delta S = X_L(c_S^{eq} - c_L^{eq})/m_L$ is the entropy change between the solid and liquid phases,
249 m_L is the liquidus slope. Eq. (20) shows two variants to calculate the driving force, first
250 in terms of the thermodynamic factors and second in terms of the difference in the en-
251 tropy (see Kundin et al. (2015), for details). Both variants are appropriate for our study.

252 $\sigma_{\beta\gamma}^*$ and $\sigma_{\alpha\gamma}^*$ are the stiffness's of the interfaces which appear due to the surface
253 energy anisotropy. We use the anisotropic model because we have to calculate highly anisotrop-
254 ically faceted crystals. The calculation of the stiffness for anisotropic faceted crystals is
255 described below.

256 By substitution of the energy functional eq. (15) in Cahn-Hilliard equation (5), one
257 obtains the diffusion equation for the concentration field

$$\frac{\partial c}{\partial t} = \nabla \cdot \left[D\nabla \frac{(c - c^{eq})}{k\phi_S + (1 - \phi_S)} + \mathbf{j}_{\mathrm{at}} \right]. \tag{21}$$

258 Here $\mathbf{j}_{\mathrm{at}}$ is the anti-trapping current, which is used for the case where the rate of diffu-
259 sion in the solid is very slow, $D = M_c X \cong (D_S\phi_S + D_L(1 - \phi_S))(k\phi_S + (1 - \phi_S))$ is the
260 mixture diffusion coefficient with D_L and D_S being the diffusion coefficients in the liq-
261 uid and solid phases, respectively, and M_c is the mixture atomic mobility.

262 ## 3.2 Modeling of the anisotropic surface energy for faceted crystals

The anisotropic surface energy is responsible for equilibrium shapes of the individ-
ual faceted crystals growing in melts and is given by the Wulff construction, which min-
imizes the total surface energy of the system. The anisotropic model used in this work
was suggested by McFadden et al. (1993) and successfully implemented by Salama et al.
(2020) for 3-D grain growth. The solid-liquid interface energy of a crystal α is defined
as a function of the inclination angle θ_α which is defined in its turn in each point of the
moving interface as an angle between the interface normal $\mathbf{n}_\alpha$ and the nearest facet nor-
mal $\mathbf{k}_{ijk}^\alpha$. The facet normals are defined at the beginning of the simulation for each par-
ticular crystal α depending on its orientation and are represented by Miller indices $\{ijk\}$.
The surface energy is then calculated by the anisotropic function of the inclination an-
gle

$$\sigma_\alpha(\theta_\alpha, (ijk)) = \sigma_{ijk}\sqrt{\sin^2(\theta_\alpha) + \kappa^2\cos^2(\theta_\alpha)}, \tag{22}$$

263 where σ_{ijk} is the maximum surface energy of a facet (ijk), κ is the anisotropy param-
264 eter which is smaller for larger anisotropy. This function produces the flat faces of crys-
265 tals which grow by propagation of planar interfaces in a manner that is different from
266 the mechanism for dendritic growth models.

The different crystal facets have different areas at equilibrium, which should be smaller
for facets with larger surface energies. That is because of the minimization of energy dur-
ing crystal growth. Furthermore, the growth rate should be faster for a facet with a larger
surface energy and smaller surfaces area. In order to capture these relationships, we de-
fine the maximum surface energy of a facet (ijk) as a function of the surface area ratio,
i. e.,

$$\sigma_{ijk} = \sigma_{001} \frac{A_{001}}{A_{ijk}}, \tag{23}$$

where A_{ijk} and A_{001} are the areas of the facets (ijk) and (001), respectively, and σ_{001}
is the maximum surface energy of the (001) facet which is used as reference energy. In
the phase-field model, the growth rate is inversely proportional to stiffness, hence we can
assume that the stiffness is directly proportional to the area of a facet. Based on this as-

sumption, we calculate the stiffness σ^* concerning the inclination angle as

$$
\begin{aligned}
\sigma_\alpha^*(\theta_\alpha, \{ijk\}) &= \frac{A_{ijk}^2}{A_{001}^2} \left(\sigma_\alpha(\theta_\alpha) + \sigma_\alpha''(\theta_\alpha) \right) \\
&= \sigma_{001} \frac{A_{ijk}}{A_{001}} \kappa^2 \left(\sin^2(\theta_\alpha) + \kappa^2 \cos^2(\theta_\alpha) \right)^{-\frac{3}{2}}.
\end{aligned}
\tag{24}
$$

Note that the assumption for the stiffness suggested here is a simplification with a clear physical meaning.

The model above is valid for single crystals in melts. To calculate the interface energy between two crystals that are in contact, we define a solid-solid interface energy $\sigma_{\alpha\beta}$ as a mean value of two solid-liquid interfaces

$$
\sigma_{\alpha\beta} = \frac{r_{sl}}{2}(\sigma_\alpha + \sigma_\beta),
\tag{25}
$$

where r_{sl} is the ratio between solid-solid and solid-liquid interface energies. Usually, the energy of solid-solid interface is larger, resulting in $r_{sl} > 1$. The stiffness for a solid-solid interface is defined than in a similar man

$$
\sigma_{\alpha\beta}^* = \frac{r_{sl}}{2}(\sigma_\alpha^* + \sigma_\beta^*).
\tag{26}
$$

In the case of small misorientation angles, the interface energy has a minimum. To mimic this behavior, we define the ratio r_{sl} for misorientations $\theta_\alpha - \theta_\beta < 5°$ equal to $r_{sl}^{\mathrm{m}} = 1$.

3.3 Evaluation of crystal size distribution (CSD)

The crystal size distribution (CSD) is defined by the number of crystals within a given size interval per unit area divided by the length interval (bin width) (Higgins, 2000, 2006), i.e.,

$$
n_V(L) = \frac{N(L_{XY})}{|L_X - L_Y|V},
\tag{27}
$$

where $N(L_{XY})$ is the total number of crystals in the simulation domain in the size interval L_X to L_Y, $|L_X - L_Y|$ is the bin width, and V is the domain volume.

The parameter $n_V(L)$ is called the population density and has units of $1/L^4$. The corresponding CSDs are usually plotted as ln(population density) versus crystal size (Marsh, 1988; Cashman, 2020).

4 Numerical results

We illustrate the capabilities of phase-field modeling using two common petrological systems – the olivine - melt system and the plagioclase - melt system. We underscore that interfacial energies playing a central role in phase-field calculations are not well known in most mineralogical systems. For illustration here, we have guessed values for the relevant energies that may yield textural appearances that correspond to those frequently observed in natural systems. The values for olivine were chosen to be in the range expected from the study of Cooper and Kohlstedt (1982). The point of this exercise is two-fold. First, to encourage the experimental measurement of the relevant parameters given the availability of this tool. Second, in natural systems where all other parameters may be independently contrained, model fits may be used to infer/constrain the values of the relevant interfacial energy parameters. The second exercise may provide a means of evaluating the range of variability of interfacial energy parameters in natural systems, and help to identify critical systems for detailed experimental studies.

4.1 Olivine – melt system

The model parameters are listed in Table 1. The calculations were carried out for for a melt of composition 73 wt.% Forsterite with a constant undercooling of 50 K (i.e. at a constant temperature of 1725° C). The diffusion coefficient is chosen as in silicate melts circa 10^{-12} m^2/s (Dingwell, 2006). The mean growth rate of olivine crystals, v_n is assumed as 10^{-5} m^2/s (Zieg & Lofgren, 2002). The interface mobility is defined at the undercooling 50 K as $\mu_{SL} = v_n/|\Delta S(T_0 - T)| \sim 10^{-13}$ m^4(Js)$^{-1}$. No flux boundary conditions in all directions are chosen for all fields. A ratio between solid-solid and solid-liquid interface energies is chosen as $r_{sl} = 1.5$. The partition coefficient is taken from (Ford et al., 1983), and the entropy and liquidus slope from MELTS.

Parameter	Symbol	Value	Units
Grid spacing	Δx	1×10^{-4}	m
Time steps	Δt	5×10^{-1}	s
Interface width	w	1.6Δx	m
Surface energy	σ_{001}	0.05	J m^{-2}
Ratio between energies	r_{sl}	1.5 and 4	-
Anisotropy strength	κ	0.2	-
Interface mobility	μ_{SL}	2.2×10^{-13}	m^4 (J s)$^{-1}$
Diffusion coefficient in liquid	D_L	3×10^{-12}	m^2 s^{-1}
Diffusion coefficient in solid	D_S	3×10^{-16}	m^2 s^{-1}
Partition coefficient	k	0.3	-
Initial concentration in melt	$C_0 = C_L^{eq}(T_0)$	73	wt. % Fo
Equilibrium concentration in melt at T	$C_L^{eq}(T)$	62	wt. % Fo
Initial concentration in nuclei	C_S^{in}	80	wt. % Fo
Equilibrium concentration in crystals	$C_S^{eq}(T)$	90	wt. % Fo
Liquidus slope	m_L	-1	K/wt%
Entropy change	ΔS	0.16	J cm^{-3} K^{-1}
Undercooling	$T_0 - T$	50	K

Table 1. Model parameters for olivine system.

4.1.1 Single olivine crystal shape

To model the shape of the real olivine crystals, we use the following surface area ratios estimated from the experimental pictures (Welsch et al., 2012)

faces	(001)	(100)	(010)	(101)	(110)	(021)
A_{ijk}/A_{001}	1	0.5	1.67	0.83	2.33	2.26

The simulated shape of a single olivine crystal is shown in Fig. 3. It is formed by using a driving force that depends on the change of the crystal volume by $\Delta G \sim (V - V_0)/V_0$, where V_0 is an initial crystal volume. An initially round crystal of radius 20Δx was placed in a cubic domain of size $66 \times 66 \times 128\Delta$x. After 2000 time steps (ts), the crystal shape transforms to the equilibrium one following the chosen anisotropic surface energy parameters. In the numerical simulations, we will use this algorithm to equilibrate the shape of nuclei before to start the main simulation runs.
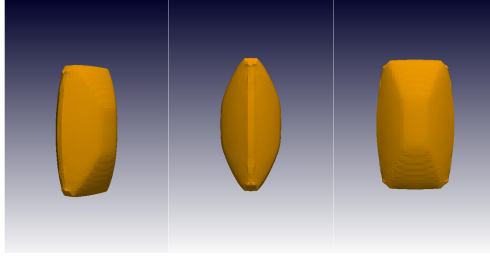
Figure 3. 3-D views of olivine crystals simulated with the (001), (010), (101), (110), and (021) faces.

4.1.2 Solidification of a system of olivine crystals

In the following, we present the simulation of the monomineralic solidification of olivine crystals in a basaltic melt. Exponential nucleation is modeled by the generation of nuclei of random sizes that are randomly distributed in space. The random size of nuclei is defined as $R_0 = (7 + 0.5 \cdot 10^{1.3\,\delta})\Delta x$, where δ is a random number from 0 to 1. This method produces an exponential distribution of nuclei which then results in a linear crystal size distribution, as used in the theoretical models of crystallization in rocks (Higgins, 2000). To avoid the contact of nuclei (pure homogeneous nucleation), the distance between the nuclei is limited to $20\Delta x$. The scheme of the phase diagram with the initial composition C_0 and the solidification temperature T_0 is shown in Fig. 4. We assume that nuclei are formed at higher undercooling, and hence they have initial compositions that are different from the equilibrium composition at temperature T.
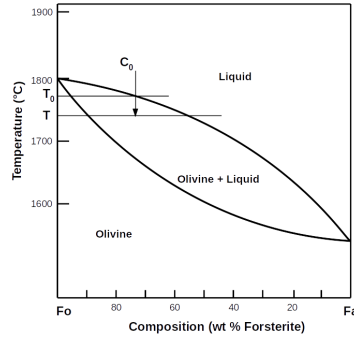

Figure 4. Phase diagram of the Fo-Fa system and the thermodynamic history used in the simulation of olivine crystals.

Simulation 1 was carried out in a cubic domain of size $186^3\Delta x$ with 320 nuclei. The simulated microstructure is shown in Fig. 5 as 3-D views at the different time steps (ts): 50 s (3000 ts), 300 s (8000 ts), and 700 s (16000 ts). The corresponding 2-D slices through the 3-D microstructure with the concentration field are shown in the second row of Fig. 5.

In Simulation 2, the system size is increased to $276^3\Delta x$ and the number of nuclei to 580. The simulated microstructure as 3-D views and 2-D slices of the concentration field is shown in Fig. 6 at different time steps. The CSDs for both tests are shown in Fig. 7. It can be seen that CSDs similarly change with time in both simulations. Hence the system size does not influence the texture. The initial number of crystals decreases dur-
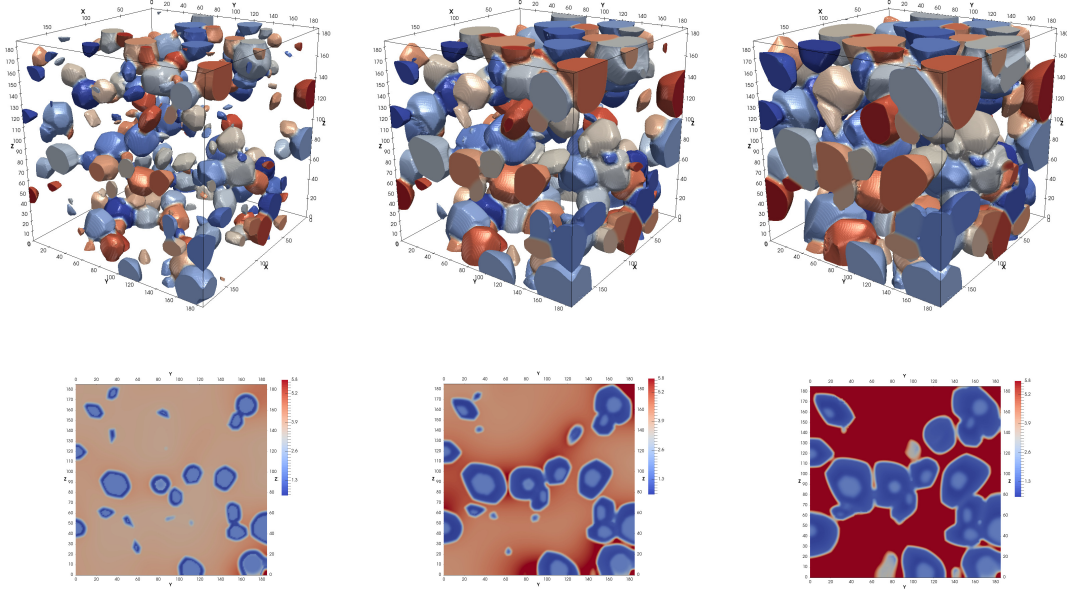
Figure 5. 3-D view of the microstructure of the olivine crystals and 2-D slices with the concentration fields of fayalite in Simulation 1 at 50 s, 300 s and 700 s. The colors represents the phase-field order parameters.

ing crystallization that results in the transformation of the exponential to a uniform distribution. This is because the growth rate depends on the crystal size and the curvature of faces. Therefore, the small crystals dissolve and the larger crystals grow faster. The time evolution of the solid phase for Simulations 1 and 2 are compared in Fig. 8. The solid fraction goes to its equilibrium value for the given undercooling. In the second test, we start with a finer solid fraction, but the slope of the time dependence is similar to the first simulation test, reflecting a similar average growth rate.

4.1.3 Effect of the solid-solid interface energy

The ratio between solid-solid and solid-liquid interface energies affects the ability of crystals to bind to each other. In order to study this behavior, we carried out the simulations in the domain size of $186^3 \Delta x$ with 480 initial nuclei of random size. The ratio between solid-solid and solid-liquid interface energies is increased to $r_{sl} = 4$. The simulated microstructure is shown in Fig. 9 at times 50 s, 300 s, and 750 s that correspond to the solid fractions 19%, 35%, and 61% respectively. The corresponding 2-D slices are shown in Fig. 9 on the bottom. The main difference with the previous simulation runs is that the crystals do not bond to each other, and a thin layer of melt of size from 4 to $5\Delta x$ remains between the crystals. The CSDs and the crystal fraction evolve with time in the same manner as in previous tests.

Future work is necessary to compare the simulated microstructures with experimental data and estimate the ratio between the solid-solid and solid-liquid interface energies. Furthermore, one should take into account the minimum interface energy at small misorientations between crystals that results in the formation of groups of intergrown crystals of the same orientation as it was observed in the work of Welsch et al. (2012).
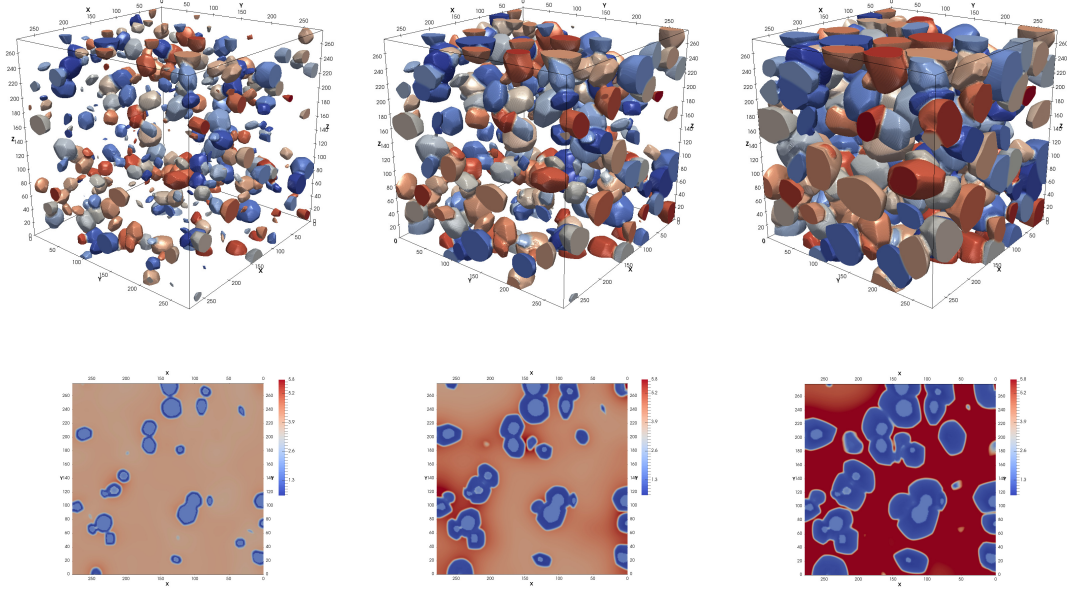
Figure 6. 3-D view of the microstructure of the olivine crystals and 2-D slices with the concentration field of fayalite in Simulation 2 at 50 s, 300 s and 700 s. The colors represents the phase-field order parameters.
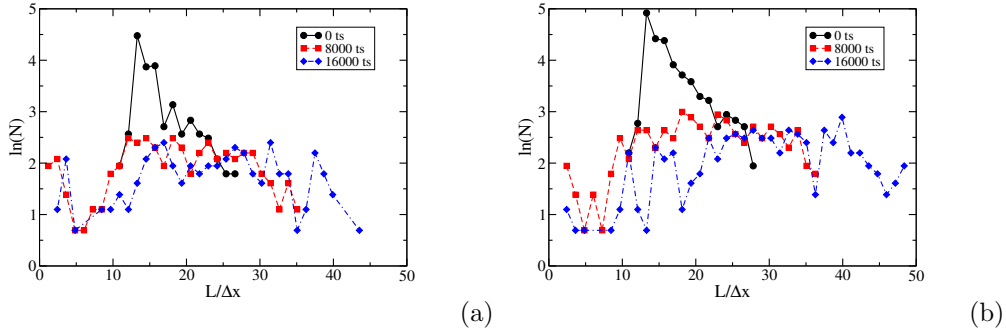

Figure 7. CSD in Simulation 1 (a), Simulation 2 (b).

4.2 Plagioclase – melt system

The model parameters that were used in the calculations are listed in Table 2. The anisotropy of the triclinic symmetry of a plagioclase crystal is modeled by two facets (100) and (001) with different surface energies. In contrast to the previous example, here we track the crystallization in the plagioclase system for a closed system with a constant bulk composition of 74 wt.%An for a constant cooling rate of 2 K/s. The numerical simulation was carried out in a rectangular domain of size $200 \times 520 \Delta x$ (2000×5200 μm). The phase diagram of the plagioclase – melt system and the initial composition are illustrated in Fig. 10. Fig. 11 shows a series of stages (abundance of phases, orientation of crystals and compositions of crystals and melt in each case) in the calculated evolution of the system for different temperatures. We introduce 44 nuclei, each 60 μm in size, at random positions in the system.
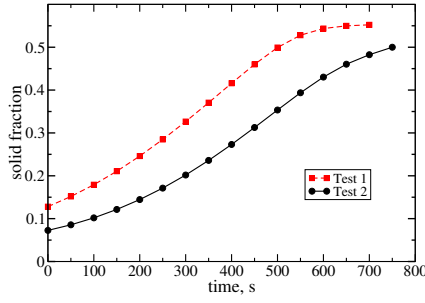
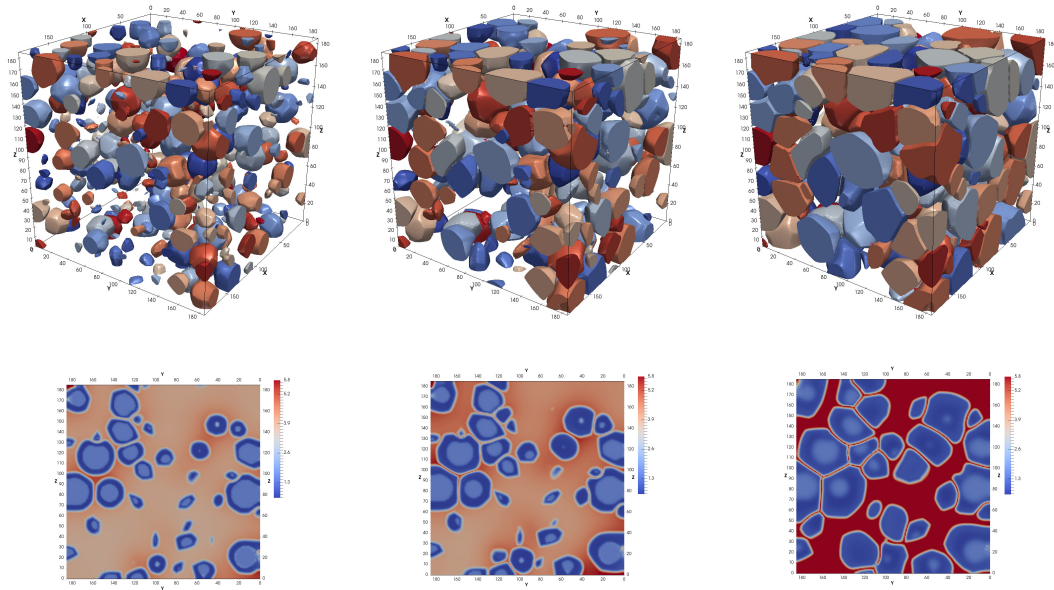**Figure 8.** Time evolution of the crystal fraction in Simulations 1, 2.

Figure 9. 3-D microstructure of the olivine crystals and 2-D slices of the olivine crystals with the concentration field at times 50 s, 300 s, and 750 s in the simulations with the large ratio $r_{sl} = 4$. The color represents the orientation of crystals.

At $T2 = 1390$°C where 13% of the system should crystallize at equilibrium, the nuclei begin to grow and the shapes of crystals (in accordance with the chosen difference in interfacial energies – see Table 2) and their compositions are shown in Fig. 11. At $T3 = 1360$°C, 28% of the system crystallizes at equilibrium, and the calculation shows growth of crystals to larger sizes. Noticeable is the fact that the composition of the liquid at a particular point in space depends on the thermodynamic (and kinetic, through diffusion) interaction with the neighbouring grains. Such interaction influences the growth rate of any given crystal and its shape. With further evolution, at $T4 = 1280$°C (68% crystallization), the growth continues and the crystal size distribution becomes more dispersed. The competition of growth between crystals produces some very large as well as some very small crystals. At $T5 = 1235$°C (90% crystallization) one has a compact crystal mush where the local compositional variation is very apparent. This has important implications for the compositions and shapes of subsequent plagioclase that grows from the
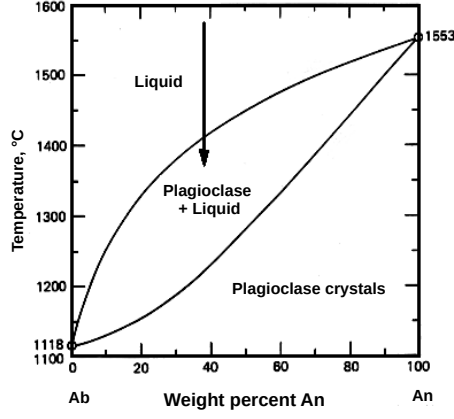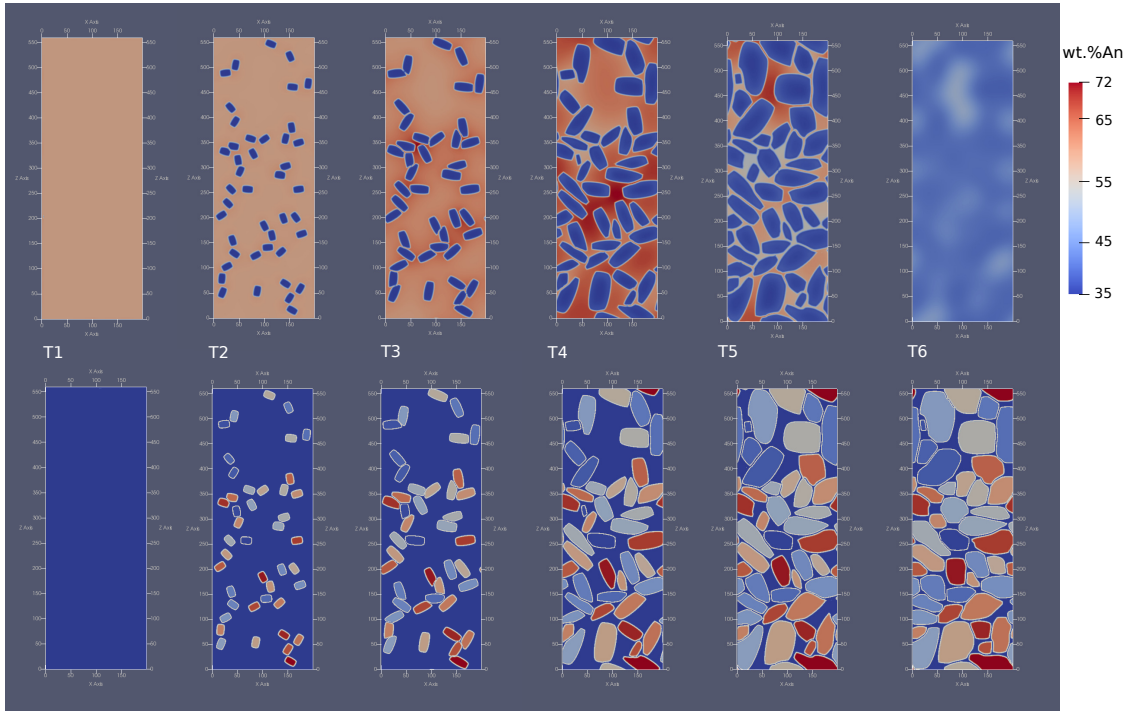
–16–

Figure 10. Plagioclase phase diagram.

Figure 11. 2-D microstructure of the plagioclase and crystals with the concentration field (top row) and phase field (bottom row) at different time steps corresponding to different temperatures during the cooling. The color represents the orientation of crystals.

melt. At $T6 = 1195°C$, the solidus is reached and there should be no remaining liquid in equilibrium. However, there is still liquid present in the simulation, which can be solidified through additional nucleation if necessary. Beyond this point, there are no significant changes in grain size of crystals but the compositions of the zoned crystals continue to evolve by diffusion. The extent of this depends obviously on the cooling rate and is an important parameter for diffusion chronometry. Fig. 12 shows the crystal size distribution in the system as the number of crystals in a size interval (one bin of the histogram equals 80 μm) in figure (a), and as crystal population density by eq. (27) in figure (b). Overall, the crystal size distribution evolves to larger sizes and becomes more

Parameter	Symbol	Value	Units
Grid spacing	Δx	1×10^{-4}	m
Time steps	Δt	5×10^{-1}	s
Interface width	w	$1.6\Delta x$	m
Surface energy	σ_{100}	1	J m^{-2}
Surface energy	σ_{001}	0.12	J m^{-2}
Ratio between energies	r_{sl}	4	-
Anisotropy strength	κ	0.2	-
Interface mobility	μ_{SL}	1×10^{-15}	m^4 (J s)$^{-1}$
Diffusion coefficient in liquid	D_L	1×10^{-9}	m^2 s^{-1}
Diffusion coefficient in solid	D_S	1×10^{-21}	m^2 s^{-1}
Initial concentration in melt	$C_0 = C_L^{eq}(T_0)$	74	wt. % An
Initial concentration in nuclei	C_S^{in}	20	wt. % An
Liquidus slope	m_L	1–2	K/wt%
Entropy change	ΔS	0.16	J cm^{-3} K^{-1}
Cooling rate	$\dot{T}$	2	K/s

Table 2. Model parameters for plagioclase – melt system

dispersed with progressive crystallization in the system. The change in crystal size distribution is a direct consequence of the competition between crystals for growth as the available volume of liquid reduces with progressive crystallization, as well as the attempt to minimize surface energies in the overall system through processes such as Ostwald ripening. During this evolution, some early formed smaller crystals disappear to enable the growth of larger crystals. Thus, the lifetime of a given crystal in the system is variable, and this aspect has important implications for diffusion chronometry.

(a)   (b)
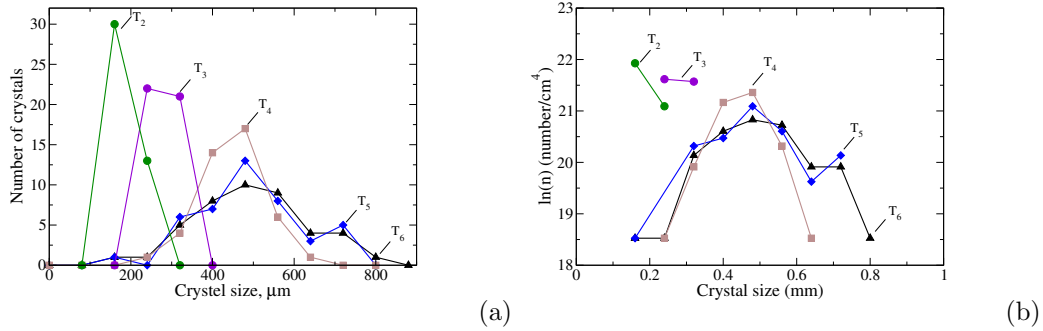
Figure 12. CSD in plagioclase system during the cooling process with linear (a) and logarithmic scale (b) on the y-axis.

Features such as the extent to which local melt compositions get trapped in growing crystals, whether they crystallize according to the locally available composition or approach the expected equilibrium composition, and whether the distribution of melts wets grain boundaries or form more isolated pockets depend on the values of the various thermodynamic and kinetic parameters and their relative magnitudes (e.g. cooling rate, interfacial energies, diffusion rates in melts, among others).

5 Discussion and conclusion

The results above demonstrate that a formal quantitative structure that permits the calculation of textural evolution taking thermodynamic constraints into account for complex, anisotropic mineralogical systems is in place. The parameters that are necessary to perform such calculations have been enumerated, and gaps in knowledge – mainly in our knowledge of various surface energy / interfacial energy parameters – have been identified. We have also outlined various approaches that may allow these quantities to be determined. This includes the possibility of documenting the distribution of grain boundaries of different orientations in natural rocks to infer the relative magnitude of anisotropy in interfacial energies in a mineral (e.g. see Marquardt et al. (2015) for the method).

A main advantage of the approach outlined here is that although nucleation behavior remains externally imposed (i.e. arbitrary), the growth rates obey local thermodynamic and geometrical constraints. Our calculations show that the form of crystal size distributions (CSD) depends on the imposed nucleation laws. However, growth in phase-field modeling results from a competition between the thermodynamic driving forces and surface energy terms that try to reduce the energetic costs of creating surfaces, particularly surfaces with higher energies (in an anisotropic system). As a result, growth rates depend on sizes of crystals and are inversely related to the curvature of a crystal surface. We note that this aspect remains irrespective of whether the growth overall is by diffusion-controlled or an interface-controlled process. The general outcome is that growth rates are not constant during the evolution of a system, and that can result in a change of slope in a CSD plot. Cashman (2020) discusses various possibilities that may give rise to such breaks in natural systems, the results obtained here provide additional alternatives. Linear CSD patterns may be expected only for limited extents of crystallization. A number of new behaviors emerge as a consequence of non-constant growth rates. For example, some smaller crystals dissolve to facilitate the growth of larger crystals (a process akin to Ostwald ripening) and growth rates react to depletion / enrichment of certain components in the melt in the immediate vicinity of a growing crystal (e.g. see Fig. 6). This extent of depletion / enrichment is controlled, in turn, by the diffusivity of the relevant elements in the melt and factors that control its physical dynamics (e.g. viscous flow, buoyancy effects) – thus, these models provide a connection between growth rates and the behavior of the melt in the system in which growth takes place. All of these aspects would influence the textural evolution of a natural system.

In the simulations in this study we produced the nuclei with considerable undercooling, so that the composition of the nuclei were far removed from the equilibrium compositions expected at the given temperature. This automatically produces compositionally zoned crystals because subsequently grown sections of the crystals form with the equilibrium compositions. The nature of such zoning is controlled by (a) the degree of undercooling, (b) the rates of diffusion of the relevant elements in the crystals, and (c) the time available for evolution (e.g. cooling rate, annealing time). These controls on the compositional zoning pattern observed in a crystal are critical inputs in diffusion chronometry but have not been explored yet in this context to any large extent. We demonstrate that phase-field modeling provides a path toward that.

Our results with different values of interfacial energies, keeping other factors the same (e.g. Fig. 9) show how melt films may separate two adjacent crystals for the certain values of this parameter. This aspect, and also the local enrichment / depletion effects discussed above, may cause a variety of different compositions to be trapped as melt inclusions in crystals growing in a closed system. In other words, external input of melt of a different composition is not necessarily required to produce melt inclusions with a wide range of compositions (see Wieser et al. (2020) for some related situations).

The phase-field simulations track the orientation of crystals of necessity, because surfaces play a central role in these calculations. Therefore, calculations such as those

shown in Fig. 6 may be used to distinguish between mush zones that have crystallized in situ, vs. cumulate piles that may have been produced by sinking crystal in a magma reservoir (e.g. see Wieser et al. (2019)). How the combination of expected compositional zoning and orientation distributions of crystals differ in those two situations would be a particularly powerful petrogenetic tool.

Finally, and perhaps most importantly from the perspective of studies of timescales of magmatic processes, this tool promises to provide a bridge between determination of timescales using CSD analysis and diffusion chronometry. Both, CSD patterns and compositional zoning patterns are calculated as part of the same internally consistent and thermodynamically valid calculation. We find, for example, that crystals do not grow monotonously since their time of nucleation. Instead, the population evolves through dissolution of some crystals and growth of others, and with different growth rates in different parts of the system. The direct consequence of this is that crystals of different sizes may have different growth zoning patterns and may have experienced diffusion for different lengths of time. The important consequence is that the lifetime of a given phase (say, olivine or plagioclase in the simulations considered in this study) in a system is different from the lifetime of a particularly crystal of the phase. In a magma reservoir residing for, say, 50 years at conditions defined by a given set of intensive thermodynamic variables (P, T, fO_2,...etc.) a phase such as olivine may be stable; but textural maturation involving dissolution and growth of crystals may have been completed much later, such that a given crystal of olivine may have been in place for, say, only 10 years. Then, 10 years is the maximum timescale that may be obtained from diffusion chronometry of olivine, using any chemical element. Thus, there is an inherent upper limit to timescales that may be accessible by diffusion chronometry of a given phase. This aspect has not been recognized yet – these simulations provide a means of exploring that limit.

Acknowledgment

References

Allen, S. M., & Cahn, J. W. (1979). A microscopic theory for antiphase boundary motion and its application to antiphase domain coarsening. *Acta Metallurgica*, *27*(6), 1085-1095. doi: 10.1016/0001-6160(79)90196-2

Amenta, R., Ewing, A., Jensen, A., Roberts, S., Stevens, K., Summa, M., ... Wertz, P. (2007). A modeling approach to understanding the role of microstructure development on crystalsize distributions and on recovering crystal-size distributions from thin slices. *American Mineralogist*, *92*(11-12), 1936–1945. doi: 10.2138/am.2007.2408

Amenta, R. V. (2001). Three-dimensional computer modeling of fabric evolution in igneous rocks. *Computers and Geosciences*, *27*(4), 477-483. (3D reconstruction, modelling and visualization of geological materials) doi: 10.1016/S0098-3004(00)00075-3

Amenta, R. V. (2004). Computer Modeling of Igneous Hypidiomorphic Textures using Crystal Prisms and Plates with Comparisons of Measured Crystal Size Distributions. In *Agu spring meeting abstracts* (Vol. 2004, p. V43C-03).

Boettinger, W. J., Warren, J. A., Beckermann, C., & Karma, A. (2002). Phase-field simulation of solidification. *Annual Review of Materials Research*, *32*(1), 163-194. doi: 10.1146/annurev.matsci.32.101901.155803

Bruno, M., Massaro, F. R., Prencipe, M., Demichelis, R., De La Pierre, M., & Nestola, F. (2014). Ab initio calculations of the main crystal surfaces of

forsterite (mg2sio4): A preliminary study to understand the nature of geo-chemical processes at the olivine interface. *The Journal of Physical Chemistry C*, *118*(5), 2498-2506.

Cahn, J. W., & Hilliard, J. E. (1958). Free energy of a nonuniform system. i. inter-facial free energy. *The Journal of Chemical Physics*, *28*(2), 258-267. doi: 10 .1063/1.1744102

Cashman, K. V. (2020). Crystal size distribution (csd) analysis of volcanic samples: Advances and challenges. *Frontiers in Earth Science*, *8*.

Chen, L.-Q. (2002). Phase-field models for microstructure evolution. *Annual Review of Materials Research*, *32*(1), 113-140. doi: 10.1146/annurev.matsci.32.112001 .132041

Cheng, M., Kundin, J., Li, D., & Emmerich, H. (2012). Thermodynamic consistency and fast dynamics in phase-field crystal modeling. *Philosophical Magazine Letters*, *92*, 517-526. doi: 10.1080/09500839.2012.691215

Cooper, R., & Kohlstedt, D. (1982). Interfacial energies in the olivine basalt system. *Journal of Fluid Mechanics*, 217–228.

de Leeuw, N. H., Parker, S. C., Catlow, C. R. A., & Price, G. D. (2000). Modelling the effect of water on the surface structure and stability of forsterite. *Physics and Chemistry of Minerals*, *27*, 332- 341.

Dingwell, D. (2006). Transport properties of magmas: Diffusion and rheology. *Elements*, *2*, 281-286. doi: 10.2113/gselements.2.5.281

Eiken, J., Böttger, B., & Steinbach, I. (2006). Multiphase-field approach for multicomponent alloys with extrapolation scheme for numerical application. *Phys. Rev. E*, *73*, 066122.

Ford, C. E., Russell, D. G., Craven, J. A., & Fisk, M. R. (1983). Olivine-Liquid Equilibria: Temperature, Pressure and Composition Dependence of the Crystal/Liquid Cation Partition Coefficients for Mg, Fe2+, Ca and Mn. *Journal of Petrology*, *24*(3), 256-266. doi: 10.1093/petrology/24.3.256

Ghiorso, M. S. (n.d.). *MELTS* [software]. Retrieved from `https://melts.ofm -research.org/`

Ghiorso, S. R. O., Mark S. (1995). Chemical mass transfer in magmatic processes IV. A revised and internally consistent thermodynamic model for the interpolation and extrapolation of liquid-solid equilibria in magmatic systems at elevated temperatures and pressures. *Contributions to Mineralogy and Petrology*, *119*, 197- 212. doi: 10.1007/BF00307281

Hersum, T., & Marsh, B. (2006). Igneous microstructures from kinetic models of crystallization. *Journal of Volcanology and Geothermal Research*, *154*, 34-47. doi: 10.1016/j.jvolgeores.2005.09.018

Hersum, T., & Marsh, B. (2007). Igneous Textures: On the Kinetics behind the Words. *Elements*, *3*(4), 247-252. doi: 10.2113/gselements.3.4.247

Higgins, M. (2000). Measurement of crystal size distributions. *American Mineralogist*, *85*(9), 1105–1116. doi: 10.2138/am-2000-8-901

Higgins, M. (2006). Verification of ideal semi-logarithmic, lognormal or fractal crystal size distributions from 2d datasets. *Journal of Volcanology and Geothermal Research - J Volcanol Geotherm Res*, *154*, 8-16. doi: 10.1016/j.jvolgeores.2005 .09.015

Hohenberg, P. C., & Halperin, B. I. (1977). Theory of dynamic critical phenomena. *Rev. Mod. Phys.*, *49*, 435–479. doi: 10.1103/RevModPhys.49.435

ICAMS, Department "Scale Bridging and Thermodynamic Simulation", Ruhr-Universtuy Bochum. (n.d.). *Openphase - the open source phase field simulation package.* Retrieved from `http://www.openphase.de/`

Karma, A. (2001). Phase-field formulation for quantitative modeling of alloy solidification. *Phys. Rev. Lett.*, *87*, 115701. doi: 10.1103/PhysRevLett.87.115701

Karma, A., & Rappel, W.-J. (1998). Quantitative phase-field modeling of dendritic growth in two and three dimensions. *Phys. Rev. E*, *57*, 4323–4349. doi: 10

.1103/PhysRevE.57.4323

Kim, H.-K., Ko, W.-S., Lee, H.-J., Kim, S., & Lee, B.-J. (2011). An identification scheme of grain boundaries and construction of a grain boundary energy database. *Scripta Materialia*, *64*, 1152-1155. doi: 10.1016/j.scriptamat.2011.03.020

Kobayashi, R. (1993). Modeling and numerical simulations of dendritic crystal growth. *Physica D: Nonlinear Phenomena*, *63*(3), 410-423. doi: 10.1016/0167-2789(93)90120-P

Kundin, J., Mushongera, L., & Emmerich, H. (2015). Phase-field modeling of microstructure formation during rapid solidification in inconel 718 superalloy. *Acta Materialia*, *95*. doi: 10.1016/j.actamat.2015.05.052

Kundin, J., & Steinbach, I. (2019). Comparative study of different anisotropy and potential formulations of phase-field models for dendritic solidification. *Computational Materials Science*, *170*, 109197. doi: 10.1016/j.commatsci.2019.109197

Langer, J. S. (1980). Instabilities and pattern formation in crystal growth. *Rev. Mod. Phys.*, *52*, 1–28. doi: 10.1103/RevModPhys.52.1

Lee, B.-J., & Choi, S.-H. (2004). Computation of grain boundary energies. *Modelling and Simulation in Materials Science and Engineering*, *12*(4), 621–632. doi: 10.1088/0965-0393/12/4/005

Lukas, H., Fries, S. G., & Sundman, B. (2007). *Computational Thermodynamics: The Calphad Method* (1st ed.). New York, NY, USA: Cambridge University Press.

Marquardt, K., Rohrer, G., Morales, L., Rybacki, E., Marquardt, H., & Lin, B. (2015). The most frequent interfaces in olivine aggregates: the gbcd and its importance for grain boundary related processes. *Contributions to Mineralogy and Petrology*, *170*. doi: 10.1007/s00410-015-1193-9

Marsh, B. D. (1988). Crystal size distribution (csd) in rocks and the kinetics and dynamics of crystallization.

McFadden, G. B., Wheeler, A. A., Braun, R. J., Coriell, S. R., & Sekerka, R. F. (1993). Phase-field models for anisotropic interfaces. *Phys. Rev. E*, *48*, 2016–2024. doi: 10.1103/PhysRevE.48.2016

Onsager, L. (1931). Reciprocal relations in irreversible processes. i. *Phys. Rev.*, *37*, 405–426. doi: 10.1103/PhysRev.37.405

Salama, H., Kundin, J., Shchyglo, O., Mohles, V., Marquardt, K., & Steinbach, I. (2020). Role of inclination dependence of grain boundary energy on the microstructure evolution during grain growth. *Acta Materialia*, *188*, 641-651. doi: 10.1016/j.actamat.2020.02.043

Saylor, D., Mason, D., & Rohrer, G. (2000). Experimental method for determining surface energy anisotropy and its application to magnesia. *Journal of the American Ceramic Society*, *83*, 1226 - 1232. doi: 10.1111/j.1151-2916.2000.tb01358.x

Spillar, V., & Dolejs, D. (2015). Heterogeneous nucleation as the predominant mode of crystallization in natural magmas: numerical model and implications for crystal–melt interaction. *Contributions to Mineralogy and Petrology*, *169*, 4.

Steinbach, I. (2009). Phase-field models in materials science. *Modelling and Simulation in Materials Science and Engineering*, *17*(7), 073001. doi: 10.1088/0965-0393/17/7/073001

Wang, S., Sekerka, R., Wheeler, A., Murray, B., Coriell, S., Braun, R., & McFadden, G. (1993). Thermodynamically-consistent phase-field models for solidification. *Physica D: Nonlinear Phenomena*, *69*, 189 – 200.

Welsch, B., Faure, F., Famin, V., Baronnet, A., & Bachèlery, P. (2012). Dendritic Crystallization: A Single Process for all the Textures of Olivine in Basalts? *Journal of Petrology*, *54*(3), 539-574. doi: 10.1093/petrology/egs077

Wieser, P. E., Edmonds, M., Maclennan, J., & Wheeler, J. (2020). Microstructural

617   constraints on magmatic mushes under kīlauea volcano, hawaii.   *Nature Com-*
618   *munications*, *11*, 14.
619 Wieser, P. E., Vukmanovic, Z., Kilian, R., Ringe, E., Holness, M. B., Maclennan,
620   J., & Edmonds, M.   (2019).   To sink, swim, twin, or nucleate: A critical
621   appraisal of crystal aggregation processes.   *Geology*, *47*(10), 948-952.   doi:
622   10.1130/G46660.1
623 Zieg, M., & Lofgren, G.   (2002).   Experimental Determination of Olivine Growth
624   Rates in Chondrules. In *Lunar and planetary science conference* (p. 1373).